Unequal layer densities in bilayer Wigner crystal at high magnetic fields

Zhihai Wang, Yong P. Chen, Han Zhu, L. W. Engel, D. C. Tsui, E. Tutuc, and M. Shayegan

Phys. Rev. B **85**, 195408 — Published 4 May 2012

DOI: 10.1103/PhysRevB.85.195408

Unequal Layer Densities in Bilayer Wigner Crystal at High Magnetic Field

Zhihai Wang,[1,2,*] Yong P. Chen,[1,3,†] Han Zhu,[1,2] L. W. Engel,[1] D. C. Tsui,[3] E. Tutuc,[2,‡] and M. Shayegan[3]

[1]*National High Magnetic Field Laboratory, 1800 E. Paul Dirac Drive, Tallahassee, FL 32310*
[2]*Department of Physics, Princeton University, Princeton, NJ 08544*
[3]*Department of Electrical Engineering, Princeton University, Princeton, NJ 08544*

(Dated: April 26, 2012)

We report studies of pinning mode resonances of magnetic field induced bilayer Wigner crystals of bilayer hole samples with negligible interlayer tunneling and different interlayer separations d, in states with varying layer densities, including unequal layer densities. With unequal layer densities, samples with large d relative to the in-plane carrier-carrier spacing a, two pinning resonances are present, one for each layer. For small d/a samples, a single resonance is observed even with significant density imbalance. These samples, at balance, were shown to exhibit an enhanced pinning mode frequency [Zhihai Wang *et al.*, Phys. Rev. Lett. 136804 (2007)], which was ascribed to a one-component, pseudospin ferromagnetic Wigner solid. The evolution of the resonance frequency and line width indicates the quantum interlayer coherence survives at moderate density imbalance, but disappears when imbalance is sufficiently large.

PACS numbers:

I. INTRODUCTION

In high magnetic field (B) two parallel layers of two-dimensional electrons in close proximity have been shown to exhibit many-body states with distinct quantum properties that arise from the degree of freedom that identifies the layer. Explicit interlayer correlations are present in the fractional quantum Hall state at total Landau level filling $\nu = 1/2$[1–5] as well as the celebrated bilayer excitonic condensate state at $\nu = 1$[4–14]. The $\nu = 1$ excitonic condensate state is seen for small layer separation and an interlayer sufficiently large that interlayer tunneling is negligible. In the well-known language in which layer index is taken as pseudospin, the state is an easy-plane ferromagnet, and has carrier wave functions coherently distributed between the two layers. Imbalance[18,19], or unequal density for the two layers has been shown[18] to strengthen the excitonic condensate state for moderate imbalance.

Bilayers, like single layer 2D carrier systems, become insulating at low enough ν, and in bilayers as in single layers[20], the low ν insulators are understood as pinned Wigner solids[15–18,21]. Several different bilayer Wigner crystal (BWC) states have been predicted theoretically[22–25] for the balanced condition, in which the carrier densities of the two layers are equal, and without interlayer tunneling (the relevant case for samples considered in this paper). These phases depend on the relative strength of interlayer and intralayer carrier-carrier interactions, as determined by d/a, where d is the interlayer separation, and $a = (\pi p_{TOT})^{-1/2}$ is the mean in-plane carrier spacing for total density p_{TOT}. For the smallest d/a, a one-component phase is predicted, which at each site of a triangular lattice has a carrier coherently present in both layers. The one-component lattice is an easy-plane pseudospin ferromagnetic BWC (FMBWC). At larger d/a, without interlayer tunneling, the phases are two-component, with each layer having a lattice. The lattices are staggered with respect to each other, so the state is a pseudospin antiferromagnetic BWC (AFMBWC). Among these two-component staggered phases, a square lattice was predicted to cover a wide range of d/a[23–25], though other phases, with rectangular or rhombic lattices, were also predicted[24,25]. For large d/a, the intralayer interaction dominates, and each layer has a triangular lattice like that of a single layer Wigner crystal.

In both single layer[26,28–30] and bilayer[31,32] systems, the spectra of the pinned low ν solid exhibit striking resonances that are understood as pinning modes, in which pieces of the solid oscillate within the potential of the residual disorder. Useful information on the pinned solid is provided by the resonance: its frequency characterizes the strength of the pinning, and its integrated amplitude indicates the number of participating carriers.

This paper expands on our earlier work[31], which exploited the pinning mode to characterize low ν BWC phases in samples at balance (with equal layer densities), using a series of p-type samples with essentially zero tunneling between layers, and different layer separations. As in the earlier paper, we use the parameter $\tilde{d} = 2^{1/2}d/a$ to characterize effective separation. The factor of $2^{1/2}$ is included in $\tilde{d}$ for comparison with the results[6,8–12] on the $\nu = 1$ excitonic Bose condensate, $\tilde{d} = d/l_{B1}$ where l_{B1} is the magnetic length at total Landau filling $\nu = 1$ for a balanced state. Our earlier paper[31] described the change in the pinning mode on changing the top and bottom layer densities, from a balanced state (p, p) to a one-layer state $(p, 0)$, in order to capture the effects of interlayer interaction and correlation on the balanced state. We found, for low interlayer separation, $\tilde{d} \leq 1.8$, that the pinning mode resonance peak frequency, $f_{\rm pk}$ was enhanced above the value expected[28] from the overall density, which determines the stiffness of the solid. We interpreted the results as consistent with these low $\tilde{d}$ samples being in an FMBWC phase at balance.

The interpretation is based on theory[33] which explains an enhancement of $f_{\rm pk}$ specific to the FMBWC, in the presence of disorder that is correlated in the two layers.

In this paper we study the same series of samples with various $\tilde{d}$, varying the layer densities to look at unbalanced states. We find that on small imbalance, the resonance does not split for samples with $\tilde{d} \leq 1.8$. For larger $\tilde{d}$, the resonance does split into two peaks, one of which is mainly sensitive to the top layer density, the other to the bottom layer density. Moreover, the $f_{\rm pk}$ enhancement observed earlier in the $\tilde{d} \leq 1.8$ at balance persists out to significant imbalance. We interpret these observations in the framework of FMBWC for low $\tilde{d}$ samples, and AFMBWC for higher $\tilde{d}$ samples. Relevant to the microwave measurements are the depths b below the sample top surface of the midpoint between the two layers, which are in all cases

Wafer Name	d (Å)	p (10^{10}cm^{-2})	$\tilde{d}$	$\nu=1$ QHE	p_B^* (10^{10}cm^{-2})
$M440$	225	3.0	1.39	yes	> 7
$M440$	225	3.85	1.57	yes	> 7
$M465$	230	3.65	1.56	yes	> 7
$M417$	260	3.05	1.61	yes	~ 4.8
$M433$	300	2.52	1.7	no	~ 4.8
$M433$	300	2.85	1.8	no	~ 4.7
$M436$	450	2.4	2.5	no	~ 1.7
$M443$	650	2.85	3.9	no	≈ 0
$M453$	2170	5.25	18	no	≈ 0

TABLE I: All the samples discussed in this paper. For each sample, interlayer separation (d), per layer density at balance (p), and $\tilde{d} \equiv d/(4\pi p)^{-1/2}$ are labeled. The samples whose balanced states show a $\nu = 1$ interlayer phase coherent quantum Hall state are marked. For bottom layer density $p_B < p_B^*$, the BWC has a single pinning mode. p_B^* is given for each sample, while for $p_B > p_B^*$, the BWC has two pinning modes (except when the bilayer is near balance, see text). The two lines each in the table for M440 and for M433 correspond to different cool downs.

II. EXPERIMENTAL METHOD

We present results from p-type GaAs/AlGaAs/GaAs double quantum wells (DQW) grown on (311)A substrates. Designed to suppress interlayer tunneling, pieces of the same wafers were studied in earlier dc measurements focusing on $\nu = 1$[12,18,34]. Table 1 summarizes the DQW dimensions and densities. $d = w + b$ is the distance between the centers of the two QW's, where b is the barrier width, and $w = 150$Å is the width of each QW in all these samples. p is the as-cooled top-layer density, taken for zero gate voltage. p_B^*, to be discussed later, is the observed bottom-layer density, above which two pinning modes can be resolved in imbalanced states. M465 and M453 are asymmetrically doped on both sides of the DQW; all other samples have dopants only at the front of the DQW. The two lines for M440 correspond to two different cool downs, each with different p. The interlayer barrier layer is AlAs for $d \leq 300$ Å, but is a combination of AlAs and AlGaAs for $d > 300$ Å.

Our microwave measuring setup has been described in earlier publications[26–30]. Figure 1 shows a schematic of a bilayer sample and the measuring circuit. A metal film transmission line on the top surface of the sample couples capacitively with the bilayer. The transmission line is of the coplanar waveguide (CPW)[35] type, with narrow, driven center conductor, separated from broad grounded side planes by slots of width W. For the measurements in this paper $W = 30\mu$m, and the depth z_0 of the bilayer center below the sample surface is between 0.72 and 0.78 μm.

In the high-frequency (f), low-loss case, the in-plane microwave electric field is well-confined to the region of bilayer immediately under the slots, so that an approximate real diagonal conductivity is given by

$$\mathrm{Re}(\sigma_{xx}) \approx -W|\ln(P/P_0)|/2Z_0L, \tag{1}$$

where P is the transmitted power, P_0 is the transmitted power for a reference state in which bilayer conductivity is zero, $Z_0 = 50\ \Omega$ is the characteristic impedance calculated from the transmission line geometry for $\sigma_{xx} = 0$, and L is the length of the line ($L = 28$ mm) for the meander CPW used in this paper. For the experiments we report, this high f, low-loss formula underestimates Re (σ_{xx}) by as much as a factor of 1.7 , relative to the more accurate model described in the next paragraph, though using the formula instead of the more elaborate model does not affect any

of the conclusions of this work or of ref. 31. A typical resonance spectrum calculated using Eq. 1 and also the more accurate model is shown in Figure 1c.

We calculate Re (σ_{xx}) data presented in this paper by modeling the fields and currents of the system of the CPW coupled to the bilayer, without requiring a high f low-loss limit. We treat the bilayer as a single layer, located at z_0 below the sample top surface. As presented in section IIIa, this approximation is verified by measurements of the most widely separated bilayer (M453), for which Re (σ_{xx}) is simply the sum of the conductivity of each layer, consistent with negligible interlayer interaction. σ_{xy} can be neglected, as verified by P reaching the same value for different IQHE plateaus, and the system is treated in the quasi-TEM approximation[36] since the width of the CPW is much less than the electromagnetic wavelength. The distributed model calculation is based on that presented by Fogler[37]. The electrostatic potential Green's function $G_{z_0}(x,x')$ for the CPW with $z = z_0$, and the potential $\phi_0(x)$ for one volt on the CPW center conductor, are found by conformal mapping, where the x axis is perpendicular to the direction of propagation of the CPW. Taking σ_{xx} to be independent of wave vector for the calculation, the potential $\phi(x)$ is found from numerical solution of

$$\phi(x) = \phi_0(x) + \frac{\sigma_{xx}}{i\omega}\int G_{z_0}(x,x')\frac{\partial^2\phi(x')}{\partial x'^2}dx'. \tag{2}$$

$\phi(x)$ is then integrated to give the nonequilibrium charge, from which we calculate the induced charge on the CPW center using Gauss' Law and the conformal mapping Green's function in the full x, z plane. We then we then calculate the per-unit-length admittance, Y_L, loading the center line of the CPW. Within the quasi-TEM approximation, Y_L, along with the σ_{xx}-independent, per-unit-length CPW series impedance Z_L, obtains characteristic impedance and propagation constant for the loaded ($\sigma_{xx} \neq 0$) CPW. From these we calculate a complex transmission coefficient s_{21} of the line using lossy transmission-line models[38]. Finally, a measured σ_{xx} is found by iteratively comparing measured $s_{21}/s_{21,0}$ (where $s_{21,0}$ is s_{21} measured for a fully depleted sample) to the calculated $s_{21}(\sigma_{xx}, f)/s_{21}(0, f)$. The data were obtained in the limit of low applied power; we verified that reducing power further did not affect the measured Re(σ_{xx}).

The samples have ohmic contacts on the edges, which connect the two layers together and allow gate biasing of the bilayer. The microwave measurement precludes a conventional front gate for independent control of top and bottom layer densities; such a gate in the slots of the coplanar waveguide would effectively short circuit the transmission line. Hence, unlike in bilayer dc transport studies such as in refs.[1,2,6–10,12,16–18], we control the layer densities only by back gate bias relative to the bilayer. One consequence of this is that the only accessible balanced state is (p,p), and it is for this state that $\tilde{d}$ is calculated.

Determination of the top and bottom layer densities p_T and p_B is based on the position and behavior of IQHE minima in Re(σ_{xx}) vs B curves taken at 200 MHz. (At that frequency, Re (σ_{xx}) is 5 μS or less, and correction between Re σ_{xx} from Eq. 1 and and the more carefully calculated Re (σ_{xx}) is around 40 %) For the smaller d samples (M440, M465, and M417), the integer quantum Hall effect (IQHE), including the $\nu = 1$ QHE, is observed for several integer total filling factors ν, allowing the total density p_{TOT} vs V_g to be obtained. The balanced condition can be found easily from the development of the $\nu = 1$ and $\nu = 2$ IQHE's , which are respectively weakest or strongest in the balanced state (p,p). p_T and p_B vs back gate voltage V_g are found using a simple capacitive model, whose main parameter, C_g, is the capacitance per unit area which relates change in p_{TOT} to a change in V_g through $\Delta p_{TOT} = C_g \Delta V_g$. In this model, both 2D layers are neglected when fully depleted but are considered as ideal conductors (large density of states) otherwise. The model has two cases: 1) $p_B > 0$, $\Delta p_B = C_g \Delta V_g$ while p_T is constant and equal to its as-cooled, unbiased value, p, and 2) $p_B = 0$ and $\Delta p_T = C_g \Delta V_g$. For the larger d samples (M433, M436, M443, and M453), the top and bottom layer densities can be derived from the positions of the IQHE minima associated with individual layers, but only for V_g ranges in which such minima are resolved. For V_g outside of these ranges, the densities are estimated by extrapolation, also based on the capacitive model.

The capacitive model neglects kinetic energy and carrier interaction in the layers. For a hole bilayer with a backgate, when p_B is nearly depleted, this can cause p_T to increase slightly with increasing V_g (or decreasing p_{TOT}), while p_B decreases faster than linearly. This deviation from the capacitive model, referred to as carrier transfer, was studied $B = 0$[39–41], and considered in the high B insulating regime[41]. Carrier transfer does not affect the relationship of p_{TOT} and V_g, and does not affect the identification of the balanced state (p,p). Following calculations in refs.[42,43], using a classical estimate of a single-layer Wigner crystal cohesive energy, and neglecting the kinetic energy since both layers are considered in the lowest Landau level, we find the capacitive model can underestimate the the p_{TOT} at which the the bottom layer is completely depleted by as much as 1×10^{10} cm^{-2}.

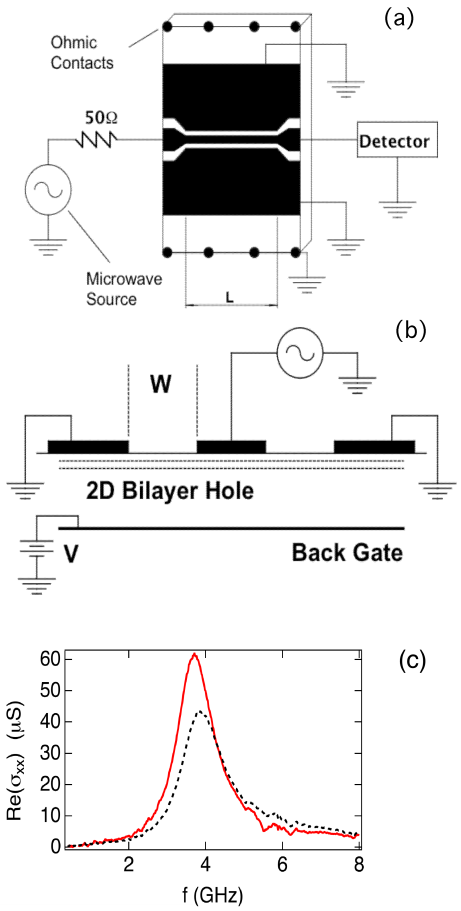

FIG. 1: Schematic representation of microwave circuit used in our measurement, not to scale. (a) top-view. Black areas represent metal films on the sample surface. (b) Side-view. Heavy black lines indicate metal film of the transmission line structure. (c) Spectra, real diagonal conductivity Re (σ_{xx}) vs frequency, f, from sample M465. The dotted line is calculated from measured data using the approximate Eq. 1. The solid line is calculated using the more elaborate method described in the text.

III. EXPERIMENTAL RESULTS

A. Large separation

For the most widely separated samples, M453 and M443, we find two resolved pinning modes whenever there is significant p_B, as long as the layer densities are not too close to balance. M453 represents the independent layer case, with $d = 2170$Å and $\tilde{d} = 18$. Figure 2a shows spectra as B increases for a state with layer densities $(p_T, p_B) = (5.3, 3.3) \times 10^{10}$ cm^{-2}. At high B, two distinct peaks are visible in the spectrum, which are labeled "T" and "B" on the graph, since they are identified with the top and bottom layers of the sample. The peaks appear as the filling factor of the respective layer goes below about 0.3, consistent with an earlier study[27] of pinning mode development in single-layer p-type samples. In the rest of this paper we are concerned only with this low ν solid regime, in which the pinning modes are well developed.

Figure 2b shows spectra of M453 at 14 T in bilayer states with fixed p_T and varying p_B, as required by the experimental constraints discussed in the previous section. The behavior is consistent with the independent layer case and with the association of each resonances with a particular layer. Resonance T remains at fixed frequency and intensity as p_B is varied, while resonance B increases in peak frequency, f_{pk} as p_B is decreased. The B resonance vanishes as p_B approaches zero, and the two resonances overlap for the balanced state.

M443 has $d = 650$ Å and $\tilde{d} = 3.9$, so its layers are more closely coupled than those of M453. Figure 3 shows a set of spectra with fixed p_T and varying p_B, for sample M443 at $B = 9$ T. Again one resonance, which we label "B", is much more sensitive to p_B, but in this case the other resonance, which we label "T", has a slight but measurable p_B dependence, demonstrating that there is at least some dynamical coupling between the layers. For $p_B < p_T$, resonance T dominates and resonance B shows as a high f shoulder.

Figure 4 summarizes the data for M453 and M443, which have well-resolved pinning modes for all significant p_B, as long as the bilayer is away from balance. The dependence of the T resonance peak frequency, f_{pk}^T, of M443 is most easily seen in the inset to Figure 4b. The evidence for coupling of the pinning modes is in the gradual decrease of f_{pk}^T as p_B is decreased over most of its range. We ascribe the sharp rise of f_{pk}^T near $p_B = 0$ on the plot to change in the top-layer density.

B. Smaller separations, transition to single pinning mode

Samples M417, M433, and M436, are in the intermediate range of $\tilde{d}$ in Table 1, and show two peaks only for p_B above a threshold value, which is denoted by p_B^* and is recorded in Table 1. The case of imbalance that is small, but sufficient ($\sim 10\%$) to resolve two resonances when they are present, can give information about the balanced states of the samples. The p_B^* column in Table 1 indicates that for such small imbalance, samples with $\tilde{d} \leq 1.8$ (including M433 and M417), keep a single pinning mode, while the samples with larger $\tilde{d}$ (including M436) show two distinct pinning modes.

C. Single pinning mode: dependence on layer densities

The smallest $\tilde{d}$ samples, M465 and M440, show only one pinning mode in all accessible bilayer states. Figure 5 shows spectra of M465 with $\tilde{d} = 1.56$, for several bilayer and single layer states, at 14 T. The spectra are offset upward for clarity, so that the lowest spectrum on the graph is for the largest p_{TOT}. The single resonance varies in peak frequency, width and intensity as p_B is increased. The resonance appears sharpest just at balance, and the peak frequency has a local maximum for p_B less than p_T.

Figure 6a shows f_{pk} and full width at half maximum, Δf, vs. p_{TOT} for the resonances of M465, at two magnetic fields (14 and 8 T). For discussion, we mark regions of p_{TOT} on the figure, as well as the balanced state p_{TOT}. For p_{TOT} in region (0), the sample has carriers only in the top layer, so $p_B = 0$, and $p_{TOT} = p_T$. In region (0) f_{pk} and Δf both increase as p_{TOT} decreases, as was seen in earlier studies of the pinning modes of single layer samples[28]. f_{pk} vs p_{TOT} in region (0) fits $f_{pk} \propto p_{TOT}^{-\gamma}$, producing the solid fit lines shown, with γ within a typical range of $0.5 \pm 10\%$, also in agreement with ref. 28.

When p_{TOT} is in region (1), f_{pk} decreases with increasing p_{TOT}, essentially extending the region (0) power law $f_{pk} \propto p_{TOT}^{-\gamma}$. The extrapolation of the power law is shown by dotted lines in Figure 6a. We do not rule out that owing to charge transfer, the system may remain a single layer with the true bottom-layer density remaining zero even through region (1), though the increase of the Δf with p_{TOT}, seen in the 8 T data, is not expected[28] for a single layer system with increasing density.

At larger p_{TOT}, f_{pk} goes through a minimum; region (2) refers to the large-p_B side of the minimum, so has f_{pk} vs p_{TOT} with positive slope. Within region (2) Δf vs p_{TOT} exhibits a local maximum. Region (3), which is characterized by f_{pk} vs p_{TOT} again decreasing, includes the balanced state. In region (3), f_{pk} is markedly "pushed up" above the curve extrapolated from region (0), while Δf shows a minimum at the balance point.

The spectra of the other low-$\tilde{d}$ samples M440 and M417 evolve similarly to those of M465, and exhibit the same regions and features in f_{pk} and Δf vs p_{TOT}.

Sample M433 has slightly larger $\tilde{d}$, which varied from 1.7 to 1.8 between two cool downs, owing to slightly different as-cooled top-layer densities. The two $\tilde{d}$ values give significantly different behavior of f_{pk} and Δf vs p_{TOT}, as shown in Figure 6b. For $\tilde{d}$ of 1.7, the intermediate positive slope region (2) of f_{pk} vs p_{TOT} is less prominent than it is for M465. Δf decreases monotonically on increasing p_{TOT}, and does not exhibit any clear feature in region (2) or at balance. For the slightly higher $\tilde{d}$ of 1.8, a region of f_{pk} vs. p_{TOT} with positive slope is not observed, so that both f_{pk} and Δf decrease monotonically on increasing p_{TOT}.

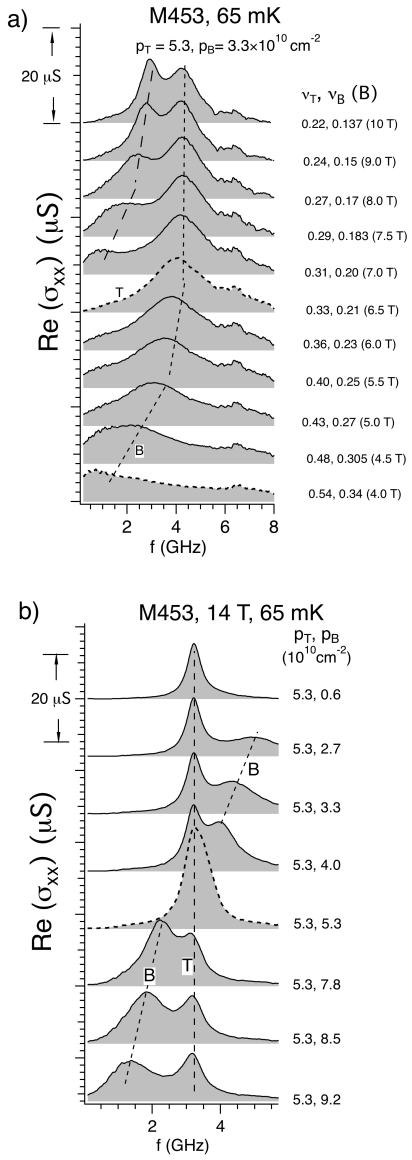

FIG. 2: (a) Spectra of M453 ($d = 2170$ Å), in a state ($p_T = 5.3, p_B = 3.3 \times 10^{10} cm^{-2}$), at several magnetic fields (B), $T \sim 65$ mK. The spectra are vertically displaced by 8 μS from each other. For each spectrum, filling factors of top and bottom layers, ν_T and ν_B, are also marked. At $\nu_T = 1/3$, or $\nu_B = 1/3$, the spectra are plotted as dashed lines. (b) Spectra of M453, in several bilayer states (p_T, p_B), at 14 T, $T \sim 65$ mK. The traces are offset by 12 μS.

IV. DISCUSSION

The interpretation of the data is in terms of two competing effects. The first effect is generic to pinning modes, including those in single layers, and is an increase of $f_{\rm pk}$ as the spacing of the interacting carriers increases. We will refer to it as the "carrier density effect", since with larger carrier-carrier spacing (smaller density) hence decreased carrier-carrier interaction, the carriers must associate more closely with the minima in the disorder potential, causing average pinning energy and average restoring force per carrier, and $f_{\rm pk}$, to increase. This behavior has been established theoretically[37,44–46] and experimentally[28] in single layers. At fixed B within the low ν carrier solid range, the experiments show $f_{\rm pk} \propto n_s^{-\gamma}$, where n_s is the single layer carrier density, and $\gamma \approx 0.5$ at low densities, but $\sim 3/2$ at higher density.

The $\gamma \approx 1/2$ power law is seen in $f_{\rm pk}$ vs p_{TOT} in regions (0) and (1) in Figure 6, and within region (3) as well. In region (1), as shown in Figure 6a, f_{pk} vs. p_{TOT} roughly follows the power law extrapolated from region (0). This behavior is explainable as due to the carrier-carrier interaction effect only and indicates that the pinning does not

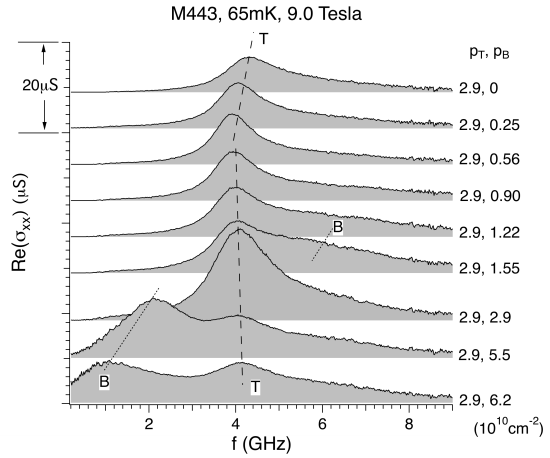

FIG. 3: Spectra of M443 in several bilayer and single layer states, at 9 T, 65 mK.

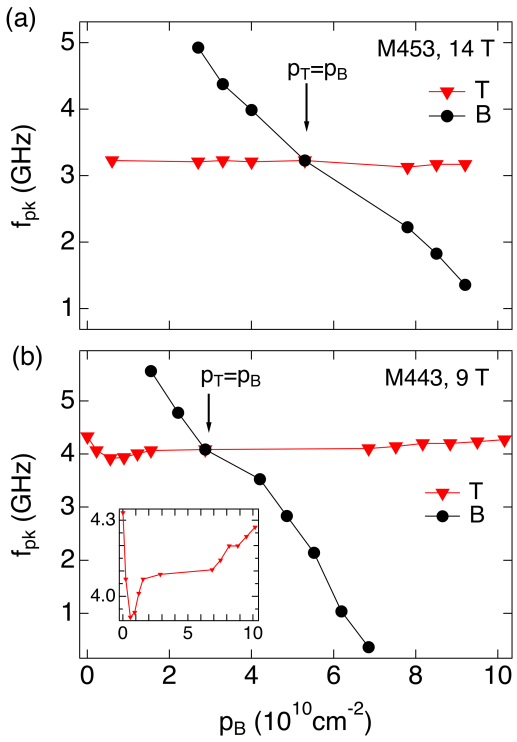

FIG. 4: (a) f_{pk}^T and f_{pk}^B (peak frequencies of resonances "T" and "B") vs p_B, for M453 ($d = 2170$ Å, $p_T = 5.3 \times 10^{10}\text{cm}^{-2}$) at 14 T. The balanced state is marked. (b) f_{pk}^T and f_{pk}^B vs p_B, for M443 ($d = 650$ Å, $p_T = 2.9 \times 10^{10} cm^{-2}$) at 9 T. The inset shows f_{pk}^T vs p_B. All data are taken at $T \sim 65$ mK.

change dramatically from the single layer condition of region 0. This suggests that the carriers do not spread between the two layers, hence the pseudospin does not have an in-plane component.

The second effect is particular to BWCs, and is an enhancement of the pinning in FMBWC relative to other BWC pseudospin orders. One of us[33] suggested that when there are positional correlations between the effective disorders in the top and bottom layers there is an enhancement of $f_{\rm pk}$ by a factor of 2 relative to the case of an AFMBWC in the low-separation limit. One possible natural source of such correlated disorder would be impurities which enable local interlayer tunneling. The amount of enhancement relative to the extrapolated carrier-density effect line was considered at balance in ref. 31. Balanced states (p, p) were compared to states $(p, 0)$ with nearly the same density in the top layer, but with the bottom layer depleted. The ratio f_{pp}/f_{p0} of the pinning mode frequencies of these states is

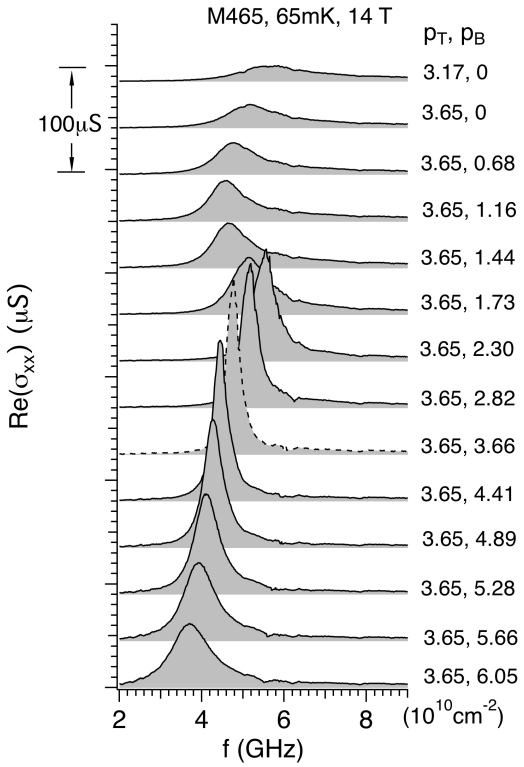

FIG. 5: Spectra of M465, in several bilayer and single layer states (p_T, p_B), at 14 T, $T \sim 65$ mK. The spectra are offset by 30 μS from each other. The spectrum at balance is plotted as a dashed line.

denoted by η, which measures the change of pinning on "adding" the bottom layer. That reference presented a curve of η vs $\tilde{d}$, which is reproduced here as Figure 6c. The curve showed a sharp minimum for $\tilde{d} \approx 1.7$. The theory[23,24] of the FMBWC for disorder-free, balanced bilayers predicts FMBWC for $\tilde{d}$ below about 0.4, considerably below the $\tilde{d}$ at which we see enhancement of pinning experimentally. One possible explanation of this discrepancy is that the FMBWC is being stabilized over competing BWC phases by its enhanced pinning.

Within region (3), for example in Figure 6a, f_{pk} decreases on increasing p_{TOT}, consistent with the carrier density effect. Overall though, f_{pk} vs. p_{TOT} in region (3) is markedly enhanced above the curve extrapolated from the single layer region (0). The upward displacement shows the pinning is enhanced relative to the pinning of single layer Wigner solid seen in region (0) and possibly region (1), after these are corrected for the carrier density effect. The enhanced pinning persists, under an imbalance $|p_T - p_B|/(p_T + p_B)$ as large as 20%. The 8 and 14 T data in Figure 6 both show the enhancement, with the 8 T enhancement slightly larger around the balanced state. This remains consistent with both fields being sufficient to produce well developed BWC solids; the differences between the 8 and 14 T curves may involve the dependence of effective disorder—which incorporates the in-plane extent of a carrier wave function—on the magnetic length[29].

The "pushed up" region (3) is observed only for states on the low $\tilde{d}$ side of the minimum in Figure 6c. We interpret the $f_{\rm pk}$ enhancement in this region as due to FMBWC formation, as was presented for the balanced case in Ref. 31, but also extending into imbalanced states. This is possible since even within an FMBWC, the carrier wave function may not spread equally in the two layers. In pseudospin language, this would also mean that at least some pseudospins have an in-plane component, and the orientation of the pseudospins changes with density imbalance. Within region (3), f_{pk} shows no sharp feature at balance, but Δf does exhibit a minimum just at balance. This suggests an imbalance-induced effect, which increases damping of the resonance without affecting pinning. Based on the classification of BWC at balance, this damping is present only when the BWC at balance is an easy-plane ferromagnet. The damping may result from excess carriers of the majority layer, which we speculate may act as defects, or could themselves form a condensed phase[47].

Region (2) can be interpreted as a transition between between region (1) with pinning of individual layers (smaller f_{pk}) and region (3) with enhanced pinning (larger f_{pk}). The local Δf maximum, which is observed in the middle of region (2), could then be interpreted as due to a transition between different BWC phases. At the transition region, multiple BWC phases can in principle coexist. The broadening effect possibly originates from dissipative excitations

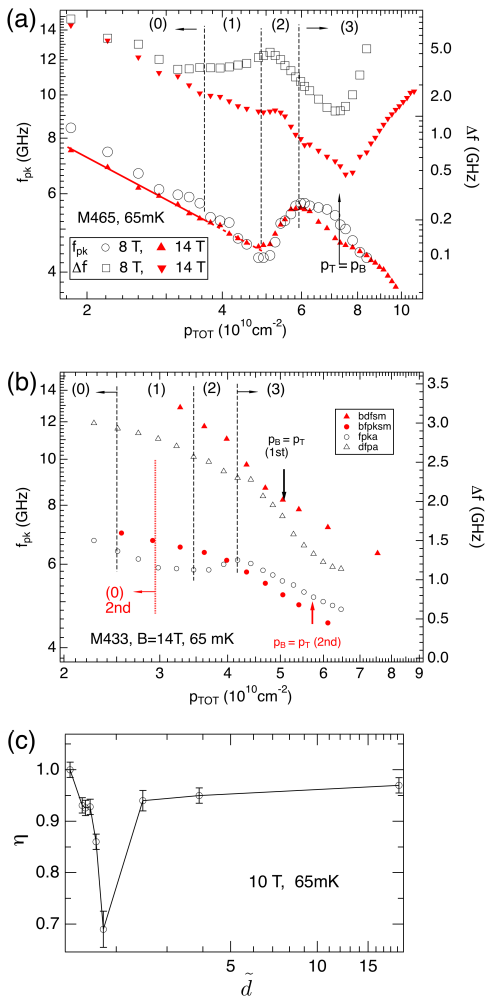

FIG. 6: (a) f_{pk} and Δf (full width at half maximum) vs total bilayer density p_{TOT}, for M465, at 8 and 14 T, $T \sim 65$ mK. In region (0), $p_B = 0$, $p_T = p_{TOT}$. On the right side of the dashed line, $p_T = 3.65 \times 10^{10}$ cm^{-2}, $p_B = p_{TOT} - p_T$. Three regions (1) - (3), separated by dashed lines, are defined according to the slope of the f_{pk} vs p_{TOT} curve. The balanced state is marked by a vertical arrow. In regions (0) and (1), f_{pk} vs p_{TOT} fits $f_{pk} \propto p_{TOT}^{-\gamma}$, with $\gamma \approx 0.5 \pm 10\%$. (b) f_{pk} and Δf vs p_{TOT}, for two cool downs of M433 ($d = 300$ Å), at 14 T, $T \sim 65$ mK. The two cool downs have different as-cooled top layer densities, leading to different $\tilde{d}$. Black, open symbols, with dashed lines separating regions: $p_T = 2.52 \times 10^{10}$ cm^{-2}, $\tilde{d} = 1.7$. Red closed symbols, with dotted lines separating regions: $p_T = 2.85 \times 10^{10}$ cm^{-2} and $\tilde{d} = 1.8$. (c) Peak frequency ratio, η, vs effective separation, $\tilde{d} \equiv d/(4\pi p)^{-1/2}$, where p is the individual layer density in the balanced state. η is the ratio of resonances frequency in the balanced state (p, p) to that in the state with the bottom layer depleted, $(p, 0)$. Based on ref 31.

.

that are associated with the phase boundaries. This picture is strengthened by the data on M433 in Figure 6b which show no local Δf maximum. For M433, which has $\tilde{d} = 1.8$, $f_{\rm pk}$ enhancement in region (3) is much less than that in M465, which has lower $\tilde{d}$. Instead, Δf for M433 decreases on increasing p_{TOT}, which can be interpreted as due to the carrier density effect.

An alternate explanation of the enhancement of $f_{\rm pk}$ around balance in region (3) in Figure 6a (and the minimum in η vs $\tilde{d}$ in Figure 6c) is that there is an increase in $f_{\rm pk}$ due to softening of the BWC. Such softening might occur around a phase transition from one type of BWC to another, since near a transition many carrier arrangements have similar energies. The Δf data in Figure 6a are difficult to reconcile to this picture, in which region (3) rather than region (2) would be identified with a transition, since the maximum in Δf occurs in region (2), and a minimum in Δf occurs in region (3). If softening of the solid occurs at a phase transition, one would naturally expect more damping at the transition, contrary to the data.

The behavior of the samples at small imbalance (small but sufficient to resolve the two pinning modes of the independent layer case) is a strong indication that a balanced sample would go though a phase transition as $\tilde{d}$ goes

below 1.8 (the minimum in Figure 6c). For $\tilde{d} \leq 1.8$ there is only one resonance at small imbalance, while for $\tilde{d} > 1.8$ the resonance splits.

In summary, by studying the peak frequency in the imbalanced states, we found that the enhanced pinning exists not only at balance, but also over a considerable range of imbalanced states (around the balance) for low-$\tilde{d}$ bilayers. In addition, the small-separation samples that show the enhanced pinning do not exhibit a splitting of the pinning mode when the layer densities are subject to small imbalance. The interpretation is in terms of a pseudospin FMBWC, present at balance but persisting even for considerable imbalance.

This work was supported by DOE Grant Nos. DE-FG21-98-ER45683 and DE-FG02-00-ER45841 at Princeton, and DE-FG02-05-ER46212 at NHMFL. NHMFL is supported by NSF Cooperative Agreement No. DMR-0084173, the State of Florida and the DOE.

---

* Current address: Riken, Advanced Science Institute, 2-1, Hirosawa,Saitama 351-0198, Japan
† Current address: Purdue University, West Lafayette, IN 47907
‡ Current address: The University of Texas, Austin, TX 78712

[1] Y. W. Suen, L. W. Engel, M. B. Santos, M. Shayegan, and D. C. Tsui, Phys. Rev. Lett. **68**, 1379 (1992); Y. W. Suen, H. C. Manoharan, X. Ying, M. B. Santos, and M. Shayegan, Phys. Rev. Lett. **72** 3405 (1994).
[2] J. P. Eisenstein, G. S. Boebinger, L. N. Pfeiffer, K. West, and S. He, Phys. Rev. Lett. **68**, 1383 (1992).
[3] B. I. Halperin, Helv. Phys. Acta **56**, 75 (1983).
[4] D. Yoshioka, A. H. MacDonald, and S. M. Girvin, Phys. Rev. B **39**, 1932 (1989).
[5] S. He, X. C. Xie, S. Das Sarma, and F. C. Zhang, Phys. Rev. B **43**, 9339 (1991).
[6] S. Q. Murphy, J. P. Eisenstein, G. S. Boebinger, L. N. Pfeiffer, and K. West, Phys. Rev. Lett. **72**, 728 (1994).
[7] T. S. Lay, Y. W. Suen, H. C. Manoharan, X. Ying, M. B. Santos, and M. Shayegan, Phys. Rev. B **50**, 17725 (1994).
[8] I. B. Spielman, J. P. Eisenstein, L. N. Pfeiffer, and K. West, Phys. Rev. Lett. **84**, 5808 (2000).
[9] I. B. Spielman, J. P. Eisenstein, L. N. Pfeiffer, and K. West, Phys. Rev. Lett. **87**, 036803 (2001).
[10] I. B. Spielman, M. Kellogg, J. P. Eisenstein, L. N. Pfeiffer, and K. West, Phys. Rev. B **70**, 081303 (2004).
[11] M. Kellogg, J. P. Eisenstein , L. N. Pfeiffer, and K. W. West, Phys. Rev. Lett. **93**, 036801 (2004).
[12] E. Tutuc, M. Shayegan, and D. A. Huse, Phys. Rev. Lett. **93**, 036802 (2004).
[13] H. A. Fertig, Phys. Rev. B **40**, 1087 (1989)
[14] A. H. MacDonald, P. M. Platzman, and G. S. Boebinger, Phys. Rev. Lett. **65**, 775 (1990).
[15] Y. W. Suen, M. B. Santos, and M. Shayegan Phys. Rev. Lett. **69**, 3551 (1992).
[16] Y. W. Suen, H. C. Manoharan, X. Ying, M. B. Santos and M. Shayegan, Surf. Sci. **305**, 13 (1994).
[17] H. C. Manoharan, Y. W. Suen, M. B. Santos, and M. Shayegan, Phys. Rev. Lett. **77**, 1813 (1996).
[18] E. Tutuc, S. Melinte, E. P. De Poortere, R. Pillarisetty, and M. Shayegan, Phys. Rev. Lett. **91**, 076802 (2003).
[19] R. D. Wiersma, J. G. Lok, S. Kraus, W. Dietsche, K. von Klitzing, D. Schuh, M. Bichler, H.-P. Tranitz, and W. Wegscheider, Phys. Rev. Lett. **93**, 266805 (2004).
[20] M. Shayegan, in *Perspectives in Quantum Hall Effects* (edited by S. Das Sarma and A. Pinczuk), 343 (Wiley Interscience, New York, 1997).
[21] S. Faniel, E. Tutuc, E. P. De Poortere, C. Gustin, A. Vlad, S. Melinte, M. Shayegan, and V. Bayot, Phys. Rev. Lett. **94**, 046802 (2005).
[22] K. Esfarjani and Y. Kawazoe, J. Phys. Condens. Matter **7**, 7217 (1995).
[23] Lian Zheng, and H. A. Fertig, Phys. Rev. B **52**, 12282 (1995).
[24] Subha Narasimhan, and Tin-Lun Ho, Phys. Rev. B **52**, 12291 (1995).
[25] G. Goldoni, and F. M. Peeters, Phys. Rev. B **53**, 4591 (1996); I. V. Schweigert, V. A. Schweigert, and F. M. Peeters, Phys. Rev. B, **60**, 14665 (1999).
[26] G. Sambandamurthy, Zhihai Wang, R.M. Lewis, Yong P. Chen, L.W. Engel, D.C. Tsui, L.N. Pfeiffer and K.W. West, Solid State Commun. **140**, 100 (2006) contains a brief review.
[27] C. C. Li, L. W. Engel, D. Shahar, D. C. Tsui, and M. Shayegan, Phys. Rev. Lett. **79**, 1353 (1997).
[28] C. C. Li, J. Yoon, L. W. Engel, D. Shahar, D. C. Tsui, and M. Shayegan, Phys. Rev. B **61**, 10905 (2000).
[29] P. D. Ye, L. W. Engel, D. C. Tsui, R. M. Lewis, L. N. Pfeiffer, and K. West, Phys. Rev. Lett. **89**, 176802 (2002).
[30] Y. P. Chen, R. M. Lewis, L. W. Engel, D. C. Tsui, P. D. Ye, Z. H. Wang, L. N. Pfeiffer, and K. West, Phys. Rev. Lett. **93**, 206805 (2004).
[31] Zhihai Wang, Yong P. Chen, L. W. Engel, D. C. Tsui, E. Tutuc, and M. Shayegan, Phys. Rev. Lett. **99**, 136804 (2007)
[32] J. B. Doveston, S. Djordjevic, R. B. Dunford, C. J. Mellor, F. I. B. Williams, M. Henini, Physica E **12** , 296 (2002).
[33] Yong P. Chen, Phys. Rev. B **73**, 115314 (2006).
[34] E. Tutuc, Ph.D Thesis, Department of Physics, Princeton University 2004.
[35] C. P. Wen, IEEE Trans. Microwave Theory Tech., **MTT-17**, 1087 (1969).
[36] A. F. dos Santos and J. P. Figanier, IEEE Trans. Microwave Theory Tech., **MTT-23**, 753 (1975).
[37] M. M. Fogler, and D. A. Huse, Phys. Rev. B **62**, 7553 (2000); M. M. Fogler, Private communication for details of the calculation for coplanar waveguide transmission in the proximity of a 2D electron system.

[38] W. Eisenstadt and Yungseon Eo, IEEE Trans. Components, Hybrids and Manufacturing Tech., **15**, 483 (1992).
[39] X. Ying, S. R. Parihar, H. C. Manoharan, and M. Shayegan, Phys. Rev. B **52**, 11611 (1995).
[40] S. J. Papadakis, J. P. Lu, M. Shayegan, S. R. Parihar, and S. A. Lyon, Phys. Rev. B **55**, 9294 (1997).
[41] J. P. Eisenstein, L. N. Pfeiffer, and K. W. West, Phys. Rev. B **50**, 1760 (1994).
[42] P. P. Ruden, and Z. Wu, Appl. Phys. Lett. **59**, 2165 (1991).
[43] Y. Katayama, D. C. Tsui, H. C. Manoharan, S. Parihar, and M. Shayegan, Phys. Rev. B **52**, 14817 (1995).
[44] H. Fukuyama, and P. A. Lee, Phys. Rev. B **18**, 6245 (1978).
[45] R. Chitra, T. Giamarchi, and P. Le Doussal, Phys. Rev. Lett. 80, 3827 (1998); R. Chitra, T. Giamarchi, and P. Le Doussal, Phys. Rev. B **65**, 035312 (2001).
[46] H. A. Fertig, Phys. Rev. B **59**, 2120 (1999).
[47] Kun Yang, Phys. Rev. Lett. **87** 056802 (2001).